coatings

MDPI

Article

Contribution of High Mechanical Fatigue to Gas Turbine Blade Lifetime during Steady-State Operation

Sung Yong Chang [1,2] and Ki-Yong Oh [3,*]

[1] Power Generation Laboratory, Korea Electric Power Corporation Research Institute, Munjiro 105, Yuseong-gu, Daejeon 34056, Korea; sy.chang@kepco.co.kr
[2] School of Advanced Materials Engineering, Chung-Nam National University, 99 DaeHak-ro, Yuseong-gu, Daejun 34134, Korea
[3] School of Energy System Engineering, Chung-Ang University, 84 Heukseok-ro, Dongjak-gu, Seoul 06974, Korea
* Correspondence: kiyongoh@cau.ac.kr; Tel.: +82-2-820-5385

Received: 12 February 2019; Accepted: 22 March 2019; Published: 31 March 2019



Abstract: In this study, the contribution of high thermomechanical fatigue to the gas turbine lifetime during a steady-state operation is evaluated for the first time. An evolution of the roughness on the surface between the thermal barrier coating and bond coating is addressed to elucidate the correlation between operating conditions and the degradation of a gas turbine. Specifically, three factors affecting coating failure are characterized, namely isothermal operation, low-cycle fatigue, and high thermomechanical fatigue, using laboratory experiments and actual service-exposed blades in a power plant. The results indicate that, although isothermal heat exposure during a steady-state operation contributes to creep, it does not contribute to failure caused by coating fatigue. Low-cycle fatigue during a transient operation cannot fully describe the evolution of the roughness between the thermal barrier coating and the bond coating of the gas turbine. High thermomechanical fatigue during a steady-state operation plays a critical role in coating failure because the temperature of hot gas pass components fluctuates up to 140 °C at high operating temperatures. Hence, high thermomechanical fatigue must be accounted for to accurately predict the remaining useful lifetime of a gas turbine because the current method of predicting the remaining useful lifetime only accounts for creep during a steady-state operation and for low-cycle fatigue during a transient operation.

Keywords: degradation; high mechanical fatigue; hot gas path components; gas turbine lifetime; gas turbine blade

1. Introduction

Gas turbines form the heart of the electric power and aerospace industries, which has prompted a large amount of research into the use of material, mechanical el, and electrical engineering for increasing their efficiency [1–3]. Significant technological advances have led to increasing operating temperatures and pressures in recent decades, enhancing the efficiency of gas turbines to over 40%. These technological advances include coatings, heat treatments, a new superalloy permitting high operating temperatures, and a new cooling system [4–11]. Specifically, an F-class gas turbine, which operates at approximately 1300 °C and a pressure ratio of 16 during full-load conditions, was developed in the late 1990s and deployed to many thermal power plants. Gas turbines of the G and J classes, which operate at approximately 1500 and 1600 °C and a pressure ratio of 21 and 23, respectively, during full-load conditions, were also developed in the early 2000s and deployed to newly constructed thermal

power plants. Power plants that deploy these high-efficiency gas turbines are currently operational and under construction.

As the operating temperature of gas turbines increases, the thermal barrier coating (TBC) laminated on the hot gas pass components (HGPCs) at the first and second stages of gas turbines [12] has received increased research attention. The blades and vanes of the third and fourth turbine stages of gas turbines are not coated because the metal superalloys used for these components can withstand the more moderate operating temperatures of the third and fourth stages without the TBC. The TBC not only permits increased gas temperatures and reduced cooling requirements but also improves fuel efficiency and reliability. It plays a critical role in protecting the substrate of the HGPCs at the first and second stages of gas turbines because the superalloy, which can withstand high temperatures of over 1500 °C, is still developing at this time. Hence, the TBC mitigates heat transfer from the coating surface of the HGPCs to the substrate of the HGPCs; the thermal gradient between the two is approximately 200 °C. Therefore, the role of the TBC suggests that the failure modes of HGPCs are different from those of the other components.

If the TBC on the HGPCs becomes damaged or cracked, the substrate starts to degrade because of creep and fatigue. In contrast to HGPCs, other components such as the third- and fourth-stage blades and vanes are affected by creep and fatigue during the entire operation, owing to lack of surface coating. Thus, coating failure accelerates HGPC degradation because the metal is directly exposed to high operating temperatures, suggesting that HGPC coatings should be carefully examined and promptly repaired.

To this end, power utility companies schedule periodic maintenance known as overhaul, during which all HGPCs are disassembled and examined by an expert system following standard maintenance guidelines for gas turbines [13–18]. The expert system evaluates the coating failure and damage of HGPCs according to three categories: normal, repair, or replace. Coating failure is one of the most important features of an overhaul because it results in a fatigue failure of the substrate. Note that creep effects on the substrate can be rejuvenated using heat treatment [19,20]; thus, fatigue damage to the metal after TBC failure is more important than creep. The overhaul procedure and failure mechanism of HGPCs clearly suggest that scheduling prompt operations and maintenances (O&M) can mitigate concerns regarding coating failure due to fatigue. Moreover, the proactive maintenance of and the accurate estimation of an HGPC lifetime is an effective way to secure the safety and reliability of HGPCs as well as decrease O&M costs. Note that power utility companies typically aim to reuse HGPCs after overhaul repairs as replacing them is more expensive.

A coating failure is mainly caused by fatigue resulting from two phenomena on the coating layers. One is rumpling caused by cyclic local volume changes [21,22] due to chemical reactions in the coating layer surfaces. Local volume changes are caused by aluminum depletion and the subsequent decomposition of the β-(Ni, Pt)Al phase in a bond coat. The other phenomenon is ratcheting [23] caused by significant variations in the operating temperature, which results in periodic thermal stress on the coating layers. This phenomenon leads to undulating interfaces between the TBC and the bond coat due to thermally grown oxide that produces undesirable cyclic failure modes when it is larger than a critical undulation amplitude [24]. In addition, creep causes the growth of an interdiffusion zone and aluminum depletion layer when coatings are exposed to constant and uniform high temperature [25–27]. However, these effects do not result in coating failures (i.e., the metal is not directly exposed to high operating temperatures owing to creep).

The effects of fatigue on gas turbine lifetime have been comprehensively studied to understand the degradation mechanisms and failure modes of HGPCs [28–31] and to assess their remaining useful lifetime (RUL) [32–34]. These studies enable one to accurately estimate the operational lifetime of HGPCs and their coating layers in a gas turbine. Hence, fatigue is nowadays considered together with creep to predict the RUL of HGPCs. Specifically, low-cycle fatigue during start, stop, and trip operations and creep during steady-state operations are accounted for by calculating the equivalent operating hours (EOHs) that determine the maintenance interval of a gas turbine. This approach

assumes that creep only affects the gas turbine lifetime during a steady-state operation, owing to the constant and uniform temperature [13–18]. However, EOHs cannot fully explain the degradation of actual service-exposed blades and vanes during an overhaul. The gap between EOHs and the scrap rate that represents the RUL of a gas turbine suggests the need to elucidate the effect of both creep and fatigue on gas turbine degradation by evaluating service-exposed blades and vanes and the operating temperature.

This is the first study to characterize the contribution of fatigue to coating degradation using laboratory experiments and an analysis of service-exposed blades and vanes. In the laboratory experiments, the effect of creep on coating failure was quantified by analyzing the roughness changes in coupon specimens, which replicate the actual coatings of blades and vanes, exposed to 8000 h of operation in a range of high, constant temperatures. In the analysis of service-exposed blades and vanes, scrapped F-class service-exposed blades and vanes were analyzed using the evolution of roughness and operational data obtained from a supervisory control and data acquisition (SCADA) system. Several factors were considered to accurately predict the RUL of a gas turbine based on the aforementioned analyses.

2. Experiments

Two experimental approaches were employed to quantify the effects of isothermal heat exposure and fatigue on coating degradation. First, coupon specimens were prepared in the laboratory. These specimens were exposed to a range of uniform high temperatures to characterize the correlation between an isothermal heat treatment and the evolution of fatigue. Second, scrap blades and vanes were analyzed by observing the evolution of the roughness and analyzing the operational data obtained from a SCADA system, including the generated power and the inlet temperature of the gas turbine. Scrapped blades and vanes were deployed in an F-class gas turbine operating at a rotating speed of 3600 rpm and inlet temperature of 1293 °C (Figure 1). The specimens were cut from a cross section of the service-exposed blade airfoil 15 mm below the top of the blade tip. The specimens were fabricated with a diameter of 30 mm and thickness of 3 mm. The roughness due to rumpling and ratcheting, which is a sensitive metric for evaluating coating fatigue failure, was measured for a quantitative comparison.

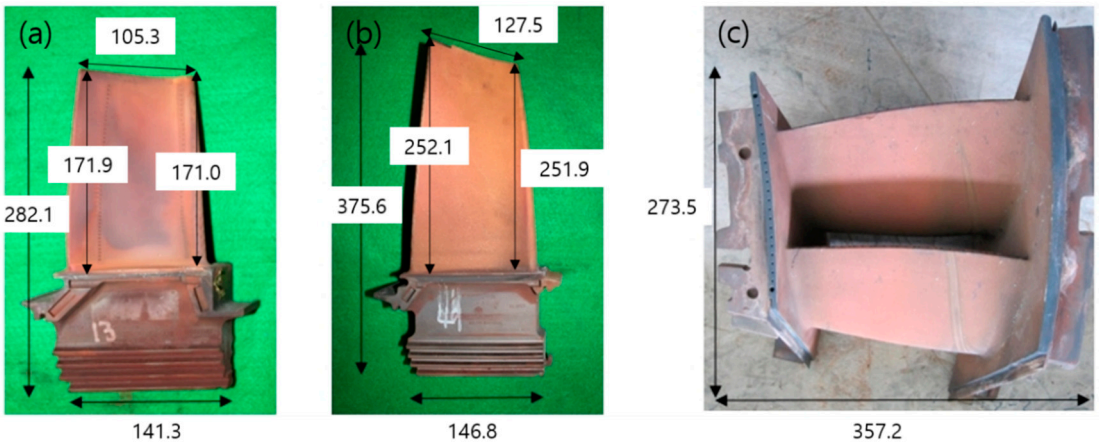

Figure 1. Service-exposed hot gas pass components (HGPCs): (**a**) first-stage blade, (**b**) second-stage blade, and (**c**) second-stage vane (unit: mm).

For the matrix of the coupon specimens in the laboratory experiments, a nickel-based directionally solidified IN738LC superalloy (nominal composition: 8.5 wt. % Co, 16 wt. % Cr, 3.4 wt. % Al, 3.4 wt. % Ti, 1.75 wt. % Mo, 2.6 wt. % W, 1.75 wt. % Ta, 0.85 wt. % Nb, 0.12 wt. % Zr, 0.012 wt. % B, 0.13 wt. % C, and the rest is Ni [35]) was cast. The specimens were cut to a diameter of 30 mm and thickness of 3 mm and prepared with the appropriate surface roughness for the adhesion of the bond and top coats by sand blasting; Sa, measured with Keyence VX-X260K (Keyence, Osaka, Japan), was less than 10.49 μm.

Atmospheric plasma spray (APS, 9M, Oerlikon Metco, Westbury, NY, USA) and low-vacuum plasma spray (LVPS, Multicoat, Oerlikon Metco, Wohlen, Switzerland), 8 wt. % Y_2O_3-ZrO_3 and NiCoCrAlY, were applied onto the IN738LC coupons as a TBC and a corrosion-resistant bond coat, respectively. The thicknesses of the TBC and bond coat (310 and 230 μm, respectively) were designed to replicate those of actual HGPCs, and these vary in the range of 250–400 and 150–300 μm, respectively depending on the manufacturer, type of components, and location, even for the same component [36].

The heat treatment of the specimens was conducted at 1120 °C for 2 h and 840 °C for 24 h in sequence. The specimens were annealed for 8000 h in a furnace at a constant temperature of 850, 950, or 1000 °C at a heating rate of 5 °C/min to quantify the effect of isothermal heat exposure on the evolution of coating fatigue.

Eight of the service-exposed blades and vanes were used to elucidate the effect of high thermomechanical fatigue as well as low-cycle fatigue and isothermal heat exposure on the blades and vanes. The blades and vanes were coated with NiCoCrAlY and stabilized zirconia after being disassembled from a W501F gas turbine at a thermal power plant in Korea, referred to as "power plant A" hereafter because of confidentiality. The blades and vanes were attached to an F-class gas turbine and were determined as fully scrapped during the overhaul by the expert system. The operational history of the blades and vanes obtained from the SCADA system are summarized in Table 1.

Table 1. The operational history of the blades and vanes scrapped from power plant A.

Sample #	Type	Stage	Equivalent Stop (ES) (h)	Operating Hours (OH) (h)	Equivalent Operating Hours (EOH) (h)
1	Blade	1st	741	14,674	29,494
2	Blade	1st	755	13,546	28,646
3	Blade	1st	232	3,248	7,888
4	Blade	2nd	1249	20,000	44,980
5	Blade	2nd	232	3,248	7,888
6	Vane	2nd	238	947	5,707
7	Vane	2nd	232	3,248	7,888

The equivalent operating hours (EOH) in Table 1 are calculated as

$$\mathrm{EOH} = 20 \times \mathrm{ES} + \mathrm{OH} \quad (1)$$

where ES and OH denote the equivalent stop and operating hours [13], respectively. The O&M guidelines of the manufacturers suggest that overhaul should be carried out to repair or replace HGPCs when an ES of 8000 h or an EOH of 24,000 h is met [14–18]. Hence, ES and EOH determines the RUL of components including HPGCs, and the period of overhaul considering two effects; ES accounts for the low-cycle fatigue during transient operations including start, stop, and trip operations, and OH accounts for the creep during steady-state operations. Note that Equation (1) is a phenomenological equation proposed by the manufacturers. The approach used by manufacturers to build Equation (1) and the values of ES and EOH that determine the RUL are strictly confidential. Hence, utility companies follow this guideline [14–18] to schedule the overhaul in general.

One important assumption in Equation (1) is that the operating temperature is constant and uniform during a steady-state operation; therefore, a steady-state operation does not contribute to fatigue. However, the failure mechanism of the HGPCs differs from that of other components, which suggests that the same formula cannot be deployed to calculate the EOH of HGPCs. As mentioned earlier, a coating failure from fatigue occurs first in HPGCs laminated using TBC and a bond coat. Once the coating is completely cracked or damaged, the metal underneath is degraded by creep and fatigue. Degradation is particularly significant in the first and second stages because the metal is exposed to high operating temperatures.

All coupon specimens and service-exposed blades/vanes were mounted and then polished with #800–#2000 SiC paper and then a vibratory polisher with alumina solutions to study their cross-sectional microstructures. The roughness of the bond coat was measured for all specimens by using an optical microscope (DM15000M, Leica, Wizlar, Germany) to quantify the fatigue due to a coating failure. Digital cross-sectional images of all the specimens were analyzed at $\times$100 magnification to calculate the roughness of the bond coat. Each image was vertically divided into 200 sections, each of which had a horizontal length of approximately 6 μm. Then, the standard deviation of the bond coat surface with respect to the mean value was measured, which is defined as the roughness hereafter, using the Leica Material workstation software (V3.6.2). Four digital images were obtained for each specimen at different locations. The standard deviations of the four digital images were averaged for an accurate estimation of the roughness of each specimen.

3. Results and Discussion

3.1. Contribution of Isothermal Heat Exposure to Fatigue

The thicknesses of the TBC and bond coat of the coupon specimens were measured 10 times via a scanning electron microscope (JSM-7001F, JEOL, Akishima, Tokyo; Figure 2) to verify that the coupon specimens were fabricated as designed. The accuracy and resolution of JSM-7001F were 0.1 and 0.01 μm, respectively. The mean thicknesses of the TBC and bond coat for one coupon specimen were 310.8 and 231.1 μm, respectively. Their respective standard deviations were 15.2 and 13.2 μm, respectively. The thicknesses of other specimens were of a similar order. A reference roughness (i.e., initial roughness) was also measured on one specimen without the isothermal heat treatment as 11.2 μm. This reference roughness (i.e., initial roughness) is shown as a green circle in Figure 3a. The initial roughness was in the preferred range of 8.9–11.4 μm for the plasma sprayed TBC performance [37], suggesting that coupon specimens could be employed to represent the coatings of blades and vanes deployed on F-class gas turbines.

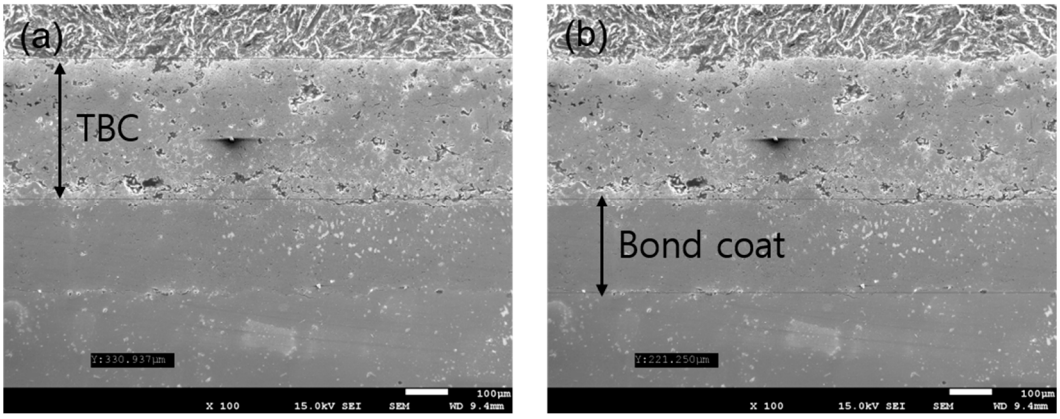

Figure 2. The scanning electron microscope images of a coated specimen: the measured thickness of (**a**) the thermal barrier coating (TBC) and (**b**) the bond coat.

The roughness of the bond coat on coupon specimens was measured to quantify the contribution of isothermal heat exposure to the evolution of fatigue. The evolution of roughness due to isothermal heat treatment is shown in Figure 3a. The square markers with a dashed line, the triangle markers with a solid line, and the circle markers with a dotted line denote the roughness at 850, 950, and 1000 °C (for 8000 h of exposure), respectively.

In Figure 3a, the roughness does not indicate any trends with isothermal heat exposure, suggesting that the isothermal heat treatment does not contribute to the rumpling and ratcheting that result in the fatigue failure of the bond coat. Specifically, an image of the bond coat surface exposed to 8000 h of heat treatment (Figure 3c) is not significantly different from that exposed to 500 h of heat treatment

(Figure 3b) at a constant temperature of 1000 °C; the roughness values on the surface between TBC and the bond coat are 11.2 and 11.4 μm, respectively. It can be deduced that the isothermal heat exposure of the blades and vanes only contributes to the degradation caused by creep. In particular, the thermally grown oxide, which is caused by the degradation due to isothermal heat exposure, is negligible in Figure 3b because the coupon specimen is only exposed for 500 h. In contrast, the thickness of thermally grown oxide is 55.3 μm when the coupon specimen is exposed for 8000 h, as shown in Figure 3c. The thickness of the thermally grown oxide is averaged 10 times, and its standard deviation is 9.0 μm. Note that fatigue, which mainly causes coating failure, is of interest in this study. Hence, thermally grown oxide representing the evolution of creep is not analyzed in detail in this study. It can be deduced that the EOH calculated by Equation (1) is reasonable if HGPCs operate only under a constant operating temperature during a steady-state operation.

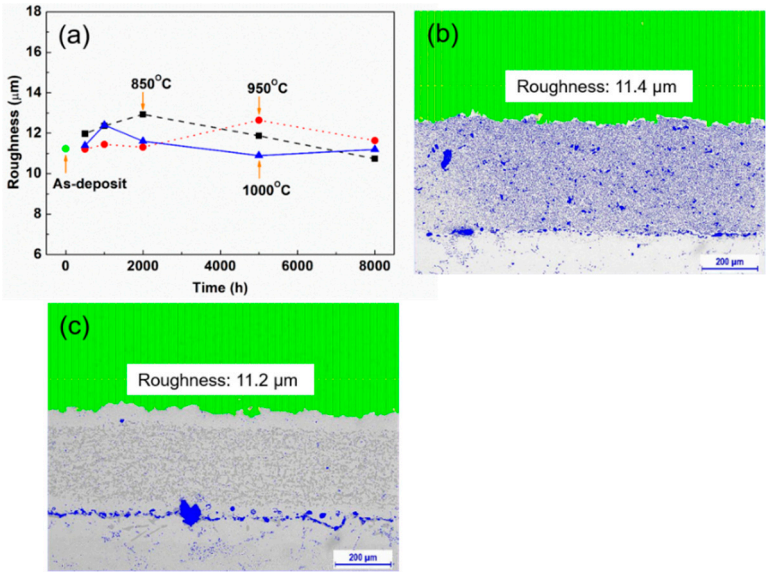

Figure 3. (**a**) The evolution of roughness on the surface between a TBC and bond coating for a variety of isothermal heat exposures and the post-processed optical microscope images representing a slight variation in the roughness on the surface between the TBC and bond coating exposed to (**b**) 500 h and (**c**) 8000 h at a constant temperature of 1000 °C.

3.2. Effects of Steady-State and Transient Operations on Fatigue

The roughness of service-exposed blades and vanes was analyzed to characterize the effect of steady-state and transient operations on the evolution of fatigue (Figure 4). The square markers with a dashed line, the triangle markers with a solid line, and the circle markers with a dotted line denote the roughness of first-stage blades, second-stage blades, and second-stage vanes, respectively.

Figure 4a shows the relationship between EOH and roughness. The roughness shows a linear dependence on EOH for all blades and vanes. Moreover, the slope of roughness with respect to EOH in the first stage is larger than that of blades and vanes exposed in the second stage, suggesting that the blades in the first stage are affected by a severe operating condition, namely a high operating temperature. These results indicate that an increase in roughness correlates directly with EOH and operating temperature. However, the limit of the result is that the contribution of a steady-state operation cannot be distinguished from that of a transient operation in these data.

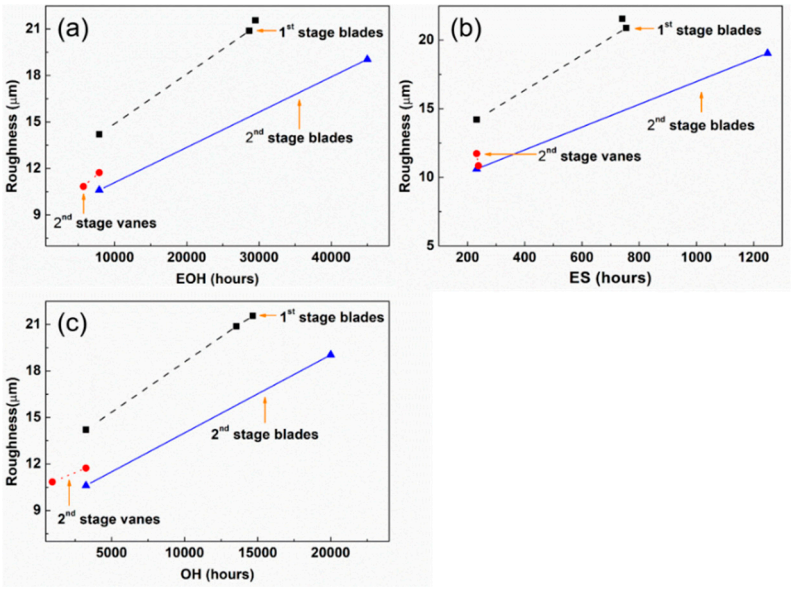

Figure 4. The controls on blade and vane roughness: The effect of (**a**) the equivalent operating hours (EOHs), (**b**) equivalent stop (ES), and (**c**) operational hours (OH) on the blade and vane roughness.

Figure 4b shows the contribution of transient operations, such as the start, stop, and trip operations, to fatigue. A low-cycle fatigue results in rumpling and ratcheting due to thermal shock loading [21,23]; therefore, the roughness should be proportional to ES. Overall, roughness should be proportional the roughness trends for all blades and vanes increase with ES. Moreover, the slope of roughness with respect to ES in the first stage is larger than that of blades and vanes exposed in the second stage, also suggesting that an increase in roughness is directly related to ES and the operating temperature. However, the roughness of the first-stage blade exposed to an ES of 741 h (sample 1) is larger than that exposed to ES of 755 h (sample 2). Although the ES of sample 1 is smaller than that of sample 2, the OH of sample 1 is larger than that of sample 2. Similarly, the roughness of the second-stage vane exposed to an ES of 232 h (sample 7) is larger than that exposed to an ES of 238 h; however, the OH of sample 7 is over three times larger than that of sample 6. These observations suggest a hypothesis that a steady-state operation can contribute to an increase in roughness: the longer the steady-state operation, the larger the roughness. However, the variation in the roughness of two vanes at the second stage is not significant, suggesting that the contribution of a steady-state operation to fatigue may be smaller than that of a transient operation.

Figure 4c shows the contribution of a steady-state operation duration to the evolution of roughness. Interestingly, the roughness of all blades and vanes increases with the number of operating hours. This result differs from the results of laboratory experiments with coupon specimens, where the roughness does not vary with the duration of the steady-state operation. There are two possibilities to explain the linear dependence of roughness on the steady-state operation. One is that power plants in Korea use a load-following mode and thereby control the power generation depending on the electricity demand. Hence, the effect of the transient response (i.e., the effect of ES) would be stochastically included in Figure 4c. The other possibility is that another reason exists for the increase in roughness during a steady-state operation. An in-depth analysis of the first hypothesis is not possible with service-exposed blades and vanes because the detailed operational history of the roughness evolution during transient and steady-state operations is not available. Regarding the second hypothesis, it is possible that the temperature is not constant during a steady-state operation. It is our view that both hypotheses contribute to the increased roughness in Figure 4c.

Figure 5 clearly shows an increase in the roughness for service-exposed blades and vanes due to fatigue. Figure 5a shows an image of the first-stage blade (sample 1 in Table 1), whereas Figure 5b shows an image of the second-stage blade (sample 4 in Table 1). The surfaces of the bond coats

are rougher than those subjected to an isothermal heat treatment (Figure 3b,c) at 21.6 and 19.0 μm, suggesting again that roughness is a sensitive metric for evaluating the evolution of fatigue.

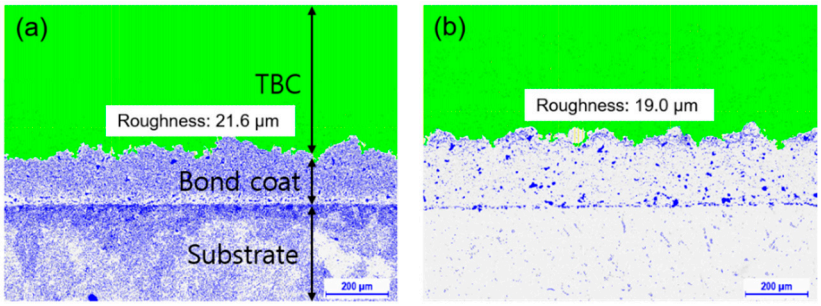

Figure 5. Post-processed optical microscope images of the bond coat surface representing a significant increase in the surface roughness compared to the fresh state (Figure 3b): (**a**) First-stage blade (sample 1 in Table 1) and (**b**) second-stage blade (sample 4 in Table 1).

To test the second hypothesis, the operating temperature of a gas turbine, which was measured from a different power plant, was analyzed. Note that the operational data is extremely difficult to obtain as these are confidential. The temperature of the steady-state operation was obtained from the SCADA system of a different power plant, referred to as "power plant B" hereafter because of confidentiality. This power plant deployed an F-class gas turbine manufactured by General Electric (GE). The total period of the obtained operational data was approximately 22 months, from 18 July 2008 to 27 May 2010. The data included the date, the generated power, and the inlet temperature at 1-h intervals. The inlet temperature of the gas turbine was calculated using the exhaust gas measured at an outlet of the gas turbine with an GE in-house code embedded in the SCADA system [19,38]. This code was developed to predict the temperature of HGPCs because the gas temperature around HGPCs is so high that it is difficult to measure. This data was fed into the SCADA system for optimal control of the power plant.

Figure 6a shows the inlet temperature with respect to the generated power. The generated power of over 150 MW is generally in a steady-state operation (inset of Figure 6a). However, the generated power in the other ranges also includes a steady-state operation because power plants in Korea have introduced a load-following mode. Hence, the inlet temperature during a steady-state operation should be separated from that during a transient operation by considering the inlet temperature over the generated power together with the operational trend. The temperature during a steady-state operation is generally in the range of 1250–1340 °C, whereas the temperature in the transient state changes over a wider range, from room temperature to 1340 °C. The maximum variation of the inlet temperature is approximately 140 °C at steady state, suggesting that temperature variations during a steady-state operation can also result in thermal stress, in addition to transient operations.

Figure 6b shows the temperature variations with 1-h intervals. Within this time interval, temperature variations above 140 °C generally occurred during transient states including the start, stop, and trip operations, whereas temperature variations below 140 °C occurred during the steady-state operation. This figure also demonstrates that the operating temperature varies even during a steady-state operation.

Figure 6c shows the temperature variations during a steady-state operation. The steady-state operation accounted for approximately 4600 h during the entire period of operation. The figure clearly shows that the inlet temperatures of the gas turbine during the steady-state operation are not constant, with a maximum variation of approximately 140 °C. Thus, it can be inferred that temperature variations during a steady-state operation contribute to rumpling and ratcheting and can contribute to thermal fatigue caused by thermal stress. Note that the coefficient of thermal expansion at a temperature of 1000 °C is 1.5 times greater than that at room temperature [39], suggesting that thermal stress during a steady-state operation also significantly affects coating degradation, although the

steady-state temperature variations are significantly smaller than those during transient operations. This high thermomechanical fatigue (HMF) observed during a steady-state operation is defined as HMF hereafter.

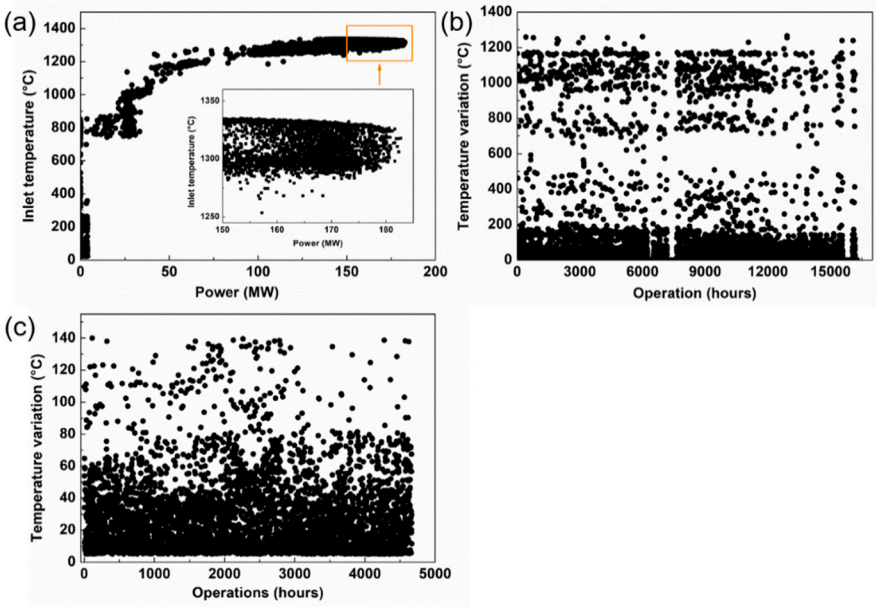

Figure 6. The temperature variation during operation: (**a**) The inlet temperature of a gas turbine against the generated power, (**b**) the variations of the inlet temperature during the entire operation, and (**c**) the variations of the inlet temperature during a steady-state operation.

In order to confirm the contribution of HMF to coating failure, additional operational data were analyzed, as presented in Table 2. These datasets were obtained from the first-stage blades in a different gas turbine in power plant B. Blade 1 and blade 2 were similarly serviced, whereas blade 3 and blade 4 were similarly serviced based on EOH. However, the scrap rate of blades 1 and 2 was different as well as that of blades 3 and 4, suggesting that EOH cannot fully account for the degradation mechanism of the HPGCs. Specifically, the scrap rate ratio of blade 4 to blade 3 was 1.10, whereas the EOH ratio of blade 4 to blade 3 was 1.01. The difference in the scrap rate could be explained by the fact that blade 4 experienced a severely transient operation (ES value in Table 2) compared to blade 3.

Table 2. The scrap rate and operational information of service-exposed blades in the gas turbines of power plant B.

Sample #	Operating Hours (OH) (h)	Equivalent Stop (ES) (h)	Equivalent Operating Hours (EOH) (h)	Scrap Rate (%)
Blade 1	10,908	376	18,428	50
Blade 2	9403	464	18,683	34
Blade 3	11,395	497	21,335	67
Blade 4	10,727	545	21,627	74

Similarly, blade 1 and blade 4 were both operated under steady state; blade 1 was used 1.6% more than blade 4. However, blade 4 was affected by long transient operation; hence, the scrap rate of blade 4 was higher than that of blade 1. These comparisons demonstrated that the thermal shock loading during a transient operation increased the coating failure and, hence, the scrap rate.

In contrast, although the EOH of blade 1 had a similar order of magnitude to that of blade 2, the scrap rate of blade 1 was higher than that of blade 2. A notable factor was that blade 1 was exposed to a shorter transient operation and a longer steady-state operation. This observation cannot be explained using the previous approach. The above comparison clearly suggests that thermal stresses

from steady-state temperature fluctuations accumulate in the coatings and contribute to coating failure. Hence, accumulated thermal stress during a steady-state operation should be accounted for when estimating fatigue lifetime to accurately predict the RUL of a gas turbine.

Our analysis of the operational data clearly demonstrates that EOH cannot fully account for the lifetime of HGPCs in a gas turbine because the coatings laminated on the surfaces of the HGPCs have different failure mechanisms compared to other components. Hence, HMF during steady state should be considered to accurately predict coating failures of HGPCs, as proposed in Figure 7. The current approach accounts for only two phenomena: low-cycle fatigue during transient states and creep during steady states. However, HMF during steady states also contributes to coating fatigue. Hence, HMF during steady states should be combined with a low-cycle fatigue to calculate the accumulated fatigue as

$$\mathrm{EOH} = \alpha \times \mathrm{ES} + \beta \times \mathrm{HMP} \quad (2)$$

where α and β denote the contribution factors of each effect.

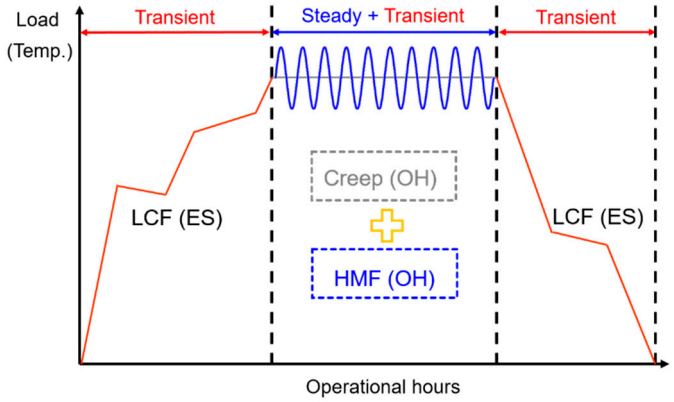

Figure 7. The proposed approach for predicting the remaining useful lifetime (RUL) and coating failure of blades and vanes in a gas turbine.

4. Conclusions

This study characterized the contribution of three factors relevant to the fatigue coating failure of HGPCs in gas turbines, which plays a critical role in the degradation of gas turbines, with the evolution of the surface roughness between the TBC and the bond coat; the factors are low-cycle fatigue during a transient operation, creep (isothermal heat exposure) during a steady state operation, and high thermomechanical fatigue during a steady state operation.

- The low-cycle fatigue during a transient operation correlated highly with the lifetime of HGPCs and linearly depended on transient operation. Hence, the current method that accounts for transient operation to evaluate the RUL of a gas turbine is reasonable.
- Isothermal heat exposure during a steady state operation slightly contributes to the RUL of HGPCs. Laboratory experiments with coupon specimens show that isothermal heat exposure does not increase roughness, although it contributes to the evolution of creep. Hence, the current method that accounts for creep during steady state to evaluate the RUL of a gas turbine should be modified.
- The high thermomechanical fatigue during a steady state operation significantly contributes to fatigue and results in coating failure as the temperature fluctuates up to 140 °C during a steady state operation, whereas the current method to evaluate the RUL of a gas turbine assumes that there is no temperature fluctuation during a steady state operation.
- The current method to evaluate the RUL of a gas turbine accounts for the high thermomechanical fatigue instead of the creep during a steady-state operation. In the future, the study should focus on calculating the thermal stress and strain during the transient state and steady state and on

evaluating the quantitative effect of HMF on coating degradation using additional long-term operational data at various operating conditions and results from laboratory experiments. A detailed phenomenological model of RUL that accounts for the effects of HMF will be developed and validated based on a quantitative analysis.

Author Contributions: Methodology, S.Y.C.; Writing—Original Draft Preparation, K.-Y.O.; Writing—Review and Editing, K.-Y.O.; Supervision, S.Y.C.

Funding: This research was supported by the National Research Foundation of Korea (NRF) grant funded by the Korea government (MEST) (No. 2017R1D1A1B03032746) and the Chung-Ang University Research Grants in 2019.

Conflicts of Interest: The authors declare no conflict of interest.

References

1. Sivakumar, R.; Mordike, B.L. High temperature coatings for gas turbine blades: A review. *Surf. Coat. Technol.* **1989**, *37*, 139–160. [CrossRef]
2. Heppenstall, T. Advanced gas turbine cycles for power generation: A critical review. *Appl. Therm. Eng.* **1998**, *18*, 837–846. [CrossRef]
3. Horlock, J.H. *Advanced Gas Turbine Cycles: A Brief Review of Power Generation Thermodynamics*; Elsevier: Amsterdam, The Netherlands, 2013.
4. Ghai, R.C.; Chen, K.; Baddour, N. Modelling thermal conductivity of porous thermal barrier coatings. *Coatings* **2019**, *9*, 101. [CrossRef]
5. Ye, D.; Wang, W.; Huang, J.; Lu, X.; Zhou, H. Nondestructive interface morphology characterization of thermal barrier coatings using terahertz time-domain spectroscopy. *Coatings* **2019**, *9*, 89. [CrossRef]
6. Guo, X.; Zhao, W.; Zeng, Y.; Lin, C.; Zhang, J. Effects of splat interfaces, monoclinic phase and grain boundaries on the thermal conductivity of plasma sprayed yttria-stabilized zirconia coatings. *Coatings* **2019**, *9*, 26. [CrossRef]
7. Lin, C.; Chai, Y.; Li, Y. Oxidation simulation of thermal barrier coatings with actual microstructures considering strength difference property and creep-plastic behavior. *Coatings* **2018**, *8*, 338. [CrossRef]
8. Manero, A.; Knipe, K.; Wischek, J.; Meid, C.; Okasinski, J.; Almer, J.; Karlsson, A.M.; Bartsch, M.; Raghavan, S. Capturing the competing influence of thermal and mechanical loads on the strain of turbine blade coatings via high energy X-rays. *Coatings* **2018**, *8*, 320. [CrossRef]
9. Dong, H.; Han, Y.; Zhou, Y.; Li, X.; Yao, J.-T.; Li, Y. The temperature distribution in plasma-sprayed thermal-barrier coatings during crack propagation and coalescence. *Coatings* **2018**, *8*, 311. [CrossRef]
10. Xiao, Y.; Ren, E.; Hu, M.; Liu, K. Effect of particle in-flight behavior on the microstructure and fracture toughness of YSZ TBCs prepared by plasma spraying. *Coatings* **2018**, *8*, 309. [CrossRef]
11. Daleo, J.A.; Ellison, K.A.; Boone, D.H. Metallurgical considerations for life assessment and the safe refurbishment and re-qualification of gas turbine blades. *J. Eng. Gas Turbines Power* **2002**, *124*, 571–579. [CrossRef]
12. Padture, N.P.; Gell, M.; Jordan, E.H. Thermal barrier coatings for gas-turbine engine applications. *Science* **2002**, *296*, 280–284. [CrossRef]
13. Janawitz, J.; Masso, J.; Childs, C. *Heavy-Duty Gas Turbine Operating and Maintenance Considerations*; GER: Atlanta, GA, USA, 2015.
14. *F-Class Combustion Turbine Life Management: Siemens V94.3A (SGT5-4000F)*; EPRI: Palo Alto, CA, USA, 2009; p. 1018614.
15. *Design Evolution, Durability, and Reliability of Alstom Heavy-Duty Combustion Turbines: Pedigree Matrices*; EPRI: Palo Alto, CA, USA, 2013; Volume 5, p. 3002001073.
16. *Design Evolution, Durability, and Reliability of Siemens Heavy-Duty Gas Turbines: Pedigree Matrices*; EPRI: Palo Alto, CA, USA, 2014; Volume 4, p. 3002006064.
17. *Design Evolution, Durability and Reliability of Mitsubishi Hitachi Heavy-Duty Gas Turbines: Pedigree Matrices*; EPRI: Palo Alto, CA, USA, 2014; Volume 7, p. 3002003863.
18. *Design Evolution, Durability and Reliability of General Electric Heavy-Duty Gas Turbines: Pedigree Matrices*; EPRI: Palo Alto, CA, USA, 2014; Volume 3, p. 3002003665.

19. Lvova, E.; Norsworth, D. Influence of service-induced microstructural changes on the aging kinetics of rejuvenated Ni-based superalloy gas turbine blades. *J. Mater. Eng. Perform.* **2001**, *10*, 299–313. [CrossRef]
20. Lvova, E. A comparison of aging kinetics of new and rejuvenated conventionally cast GTD-111 gas turbine blades. *Mater. Eng. Perform.* **2007**, *16*, 254–264. [CrossRef]
21. Tolpygo, V.K.; Clarke, D.R. Surface rumpling of A (Ni, Pt) Al bond coat induced by cyclic oxidation. *Acta Mater.* **2000**, *48*, 3283–3293. [CrossRef]
22. Panat, R.; Zhang, S.; Hsia, K. Bond coat surface rumpling in thermal barrier coatings. *Acta Mater.* **2003**, *51*, 239–249. [CrossRef]
23. He, M.Y.; Evans, A.G.; Hutchinson, J.W. The ratcheting of compressed thermally grown thin films on ductile substrates. *Acta Mater.* **2000**, *48*, 2593–2601. [CrossRef]
24. Im, S.H.; Huang, R. Ratcheting-inducted wrinkling of an elastic film on a metal layer under cyclic temperatures. *Acta Mater.* **2004**, *52*, 3707–3719. [CrossRef]
25. Anton, R.; Bkrkner, J.; Czech, N.; Stamm, W. Degradation of advanced MCrAlY coatings by oxidation and interdiffusion. *Mater. Sci. Forum* **2001**, *369*, 719–726. [CrossRef]
26. Viswanathan, R.; Cheruvu, N.S.; Chan, K.S. Coatings for Advanced Large Frame Combustion Turbines for Power Generation. In Proceedings of the ASME Turbo Expo 2003, Atlanta, GA, USA, 16–19 June 2003.
27. Kiruthika, P.; Makineni, S.K.; Srivastava, C.; Chattopadhyay, K.; Paul, A. Growth mechanism of the interdiffusion zone between platinum modified bond coats and single crystal superalloys. *Acta Mater.* **2016**, *105*, 438–448. [CrossRef]
28. Carter, T.J. Common failures in gas turbine blades. *Eng. Fail. Anal.* **2005**, *12*, 237–247. [CrossRef]
29. Mazur, Z.; Ramirez, A.L.; Islas, J.A.J.; Amezcua, A.C. Failure analysis of a gas turbine blade made of Inconel 738LC alloy. *Eng. Fail. Anal.* **2005**, *12*, 474–486. [CrossRef]
30. Vardar, N.; Ekerim, A. Failure analysis of gas turbine blades in a thermal power plant. *Eng. Fail. Anal.* **2007**, *14*, 743–749. [CrossRef]
31. Poursaeidi, E.; Aieneravaie, M.; Mohammadi, M.R. Failure analysis of a second stage blade in a gas turbine engine. *Eng. Fail. Anal.* **2008**, *15*, 1111–1129. [CrossRef]
32. Chan, K.S.; Cheruvu, N.S.; Leverant, G.R. Predicting Coating Degradation Under Variable Peak Temperatures. In Proceedings of the ASME Gas Turbine & Aeroengine Congress & Exhibition, Indianapolis, IN, USA, 7–10 June 1999.
33. Cheruvu, N.S.; Chan, K.S.; Viswanathan, R. Evaluation, degradation and life assessment of coatings for land-based combustion turbines. *Energy Mater.* **2006**, *1*, 33–47. [CrossRef]
34. Chan, K.S.; Cheruvu, S. Field Validation of a TBC Life-Prediction Model for Land-Based Gas Turbines. In Proceedings of the ASME Turbo Expo 2010, Scotland, UK, 14–18 June 2010.
35. Ellison, K.A.; Daleo, J.A.; Hussain, K. A New Method of Metal Temperature Estimation for Service-Run Blades and Vanes. In Proceedings of the 10th International Symposium on Superalloys 2000, Champion, IL, USA, 17 September 2000; pp. 759–768.
36. Smith, J.; Scheibel, J.; Classes, D.; Paschke, S.; Elbel, S.; Fick, K.; Carlson, D. Thermal barrier coating validation testing for industrial gas turbine combustion hardware. *J. Eng. Gas Turbines Power* **2016**, *138*, 031508. [CrossRef]
37. *Combustion Turbine Repair Guidelines: Hot Section Coatings, Hot Section Coatings*; EPRI: Palo Alto, CA, USA, 2010; Volume 7, p. 1022336.
38. Kniat, J. Means for Calculating Turbine Inlet Temperature of a Gas Turbine Engine. U.S. Patent 4055997A, 1 November 1977.
39. *Life Management System for Advanced F Class Gas Turbines: Siemens-Westinghouse W501F*; EPRI: Palo Alto, CA, USA, 2005; p. 1008319.



© 2019 by the authors. Licensee MDPI, Basel, Switzerland. This article is an open access article distributed under the terms and conditions of the Creative Commons Attribution (CC BY) license (http://creativecommons.org/licenses/by/4.0/).